COMPARISON OF THREE COMBUSTION MODELS FOR SIMULATING ANODE BAKING FURNACES

François Grégoire[1,2], Louis Gosselin[1,2*]

[1]Department of Mechanical Engineering, Université Laval, Québec City, Québec, Canada

[2]Aluminium Research Centre - REGAL

Article accepté pour publication dans: International Journal of Thermal Sciences, Volume 129, Juillet 2018

Abstract

Carbon anode blocks used in the Hall-Héroult process for primary aluminum production have to be baked up to 1100°C in dedicated furnaces. These furnaces are equipped with burner ramps to heat the air circulating in the flues at 1200°C, so that the anodes reach the required temperature. It is therefore mandatory to include the heat provided by the burners in a numerical model of an anode baking furnace. In this work, we modeled the heat input at the burners in three ways: the Eddy-Dissipation model, the Mixture Fraction/PDF approach and a simplified approach consisting in injecting an equivalent calorific value at the burners' inlets. Results obtained with the first two models are very similar in terms of anode baking prediction but slightly different in terms of flame temperature prediction. Results obtained with the simplified approach show that the model can replace combustion model to predict anode baking, but calibration of boundary conditions is necessary in order to match more elaborate combustion models. The importance of other elements of the model in the flue channel of the furnace has been verified: radiation (cannot be ignored, large influence on the spatial temperature distribution), heat transfer due to species diffusion (negligible influence on the baking, but slight effect on flame shape and temperature), and buoyancy (no significant effect on the results in the furnace firing sections).

Keywords: Hall-Héroult process; Anode baking; Furnace; Combustion models

Nomenclature

a to j	Molar coefficients
A	Constant of the Eddy-Dissipation model
C_1, C_2	Turbulence model coefficient and constant, respectively

* Corresponding Authors: Louis.Gosselin@gmc.ulaval.ca; Tel.: +1-418-656-7829; Fax: +1-418-656-7415.

C_d, C_g	Mixture fraction model constants
C_p	Heat capacity [J kg^{-1} K^{-1}]
$D_{i,m}$	Diffusion coefficient of species *i* in mixture [m^2 s^{-1}]
f, f'^2	Mixture fraction, mixture fraction variance
g	Gravitational acceleration [m s^{-2}]
h, h_i, h_s, $h_{s,i}$, $h^0_{f,i}$	Enthalpy [J kg^{-1}]
I	Radiative intensity [W m^{-2} sr^{-1}]
k	Turbulent kinetic energy [J kg^{-1} or m^2 s^{-2}]
$\dot{m}$	Mass flow rate [kg s^{-1}]
M	Molecular weight [g mol^{-1}]
p	Pressure [Pa]
P_k, P_b	Turbulent kinetic energy source terms [kg m^{-1} s^{-3}]
Pr_t	Turbulent Prandtl number
Q	Heat of reaction [J kg^{-1}]
$\dot{Q}$	Source term [W m^{-3}]
$\vec{r}$	Position vector
R	Reaction rate [kg m^{-3} s^{-1}]
R_u	Universal gas constant [J mol^{-1} K^{-1}]
$\vec{s}$	Unit direction vector
S	Modulus of the mean rate-of-strain tensor [s^{-1}]
Sc_t	Turbulent Schmidt number
u	Velocity components [m s^{-1}]
t	Time [s]
T, T_{ref}	Temperature [°C]
x	Cartesian coordinates [m]
X	Heating value [J kg^{-1}]
y	Mass fraction

Greek letters

δ_{ij}	Kronecker delta

ε	Dissipation rate of turbulent energy [$m^2\ s^{-3}$]
κ	Absorption coefficient [m^{-1}]
μ	Dynamic viscosity [Pa s]
μ_t	Turbulent viscosity [Pa s]
ν	Kinematic viscosity [$m^2\ s^{-1}$] or stoichiometric coefficient
ρ	Density [$kg\ m^{-3}$]
σ	Stefan-Boltzmann constant [$W\ m^{-2}\ K^{-4}$]
σ_k, σ_ε	Turbulence model constants
σ_t	Mixture fraction model constant
Ω	Control angle [sr]

Subscripts

coarse	Refers to coarse mesh
comb	Refers to combustion
fine	Refers to fine mesh
i, j	Species
i, j, l	Refers to cartesian coordinates *x*, *y* or *z*
rad	Refers to radiation

1. Introduction

According to the International Aluminum Institute, the global primary aluminum industry produced approximately 50 million metric tons of new aluminum in 2013. All of this production is achieved with the Hall-Héroult process, the most efficient version of which relies on the use of prebaked carbon anode blocks within electrolysis cells operating at about 960°C. In short, the dissolved alumina (Al_2O_3) in the cell reacts with the carbon of the anode blocks to form CO and CO_2, and as a result, pure aluminum is obtained. Therefore, the aluminum industry is constantly consuming carbon in order to produce aluminum. A typical carbon consumption rate is 0.5 ton for each ton of aluminum produced, representing approximately 15 to 20 % of the overall production costs of an aluminum smelter [1].

The carbon anode quality is of prime importance for the profitability of an aluminum plant. Variability of key anode properties such as density, electrical resistivity, permeability, thermal

shock resistance and mechanical strength have a profound influence on the stability and the costs of the electrolysis process. For example, a higher anode permeability will increase the transport of oxidant gases (air and CO_2) within the anode matrix, therefore increasing the anode consumption in the electrolysis cell, resulting in a shorter anode lifetime and higher carbon consumption [2]. Aluminum smelters are continuously seeking for new ways to improve anode fabrication, from the supply of raw materials to the optimization of the different production steps.

Prior to their use in an electrolysis cell, the carbon anode blocks are fabricated in 4 main steps. First, the paste production consists in the mixing of raw materials, the typical recipe being 65 % petroleum coke, 15 % binder pitch and 20 % recycled anode butts. The next step is to form the mixed paste into blocks by moulding or vibrocompaction, resulting in what are called green anodes. The third step consists in baking the anodes in a furnace where they will reach a maximum temperature of about 1100°C in order to acquire adequate chemical, electrical, mechanical and thermal properties. Finally, the last sept of the anode fabrication is the rodding, which consists in equipping the baked anodes with an assembly that enables the carbon blocks to be held in cells and through which the electric current passes.

The baking of the anodes is the most expensive and the most energy-consuming step of the anode fabrication process [1]. The anodes are baked in large furnaces that steadily burn natural gas (or oil) to generate enough heat for the baking process to take place. The energy efficiency of anode baking furnaces (ABF) is a primary concern in the aluminum industry, typically expressed in the amount of energy that an ABF consumes per ton of baked anodes produced (GJ/ton). Recent furnaces consume about 2 GJ/ton [1]. In addition to energy consumption, the ABFs constantly need to be serviced with new refractories and cleaned between baking cycles so that the baking process remains uniform and safe.

Numerical modeling of the anode baking process started in the early 1980s. The need for numerical models came naturally since proceeding by ‘trial and error’ experiments on a furnace is time and resource consuming due to the length of the baking cycle and the severe temperature conditions in the furnace. Moreover, the quality of several hundreds of anodes could be jeopardized with in-situ optimization of a furnace. Complexity and applications of ABF numerical models vary a lot, but they can be separated in two main categories: process models and design models.

The application of process models is to predict the overall conditions in the furnace during an entire baking cycle. These models are one or two-dimensional and they essentially solve momentum and energy balances along the flue channel, accompanied by the conduction equation in a certain number of slices of the solids (anodes, coke, refractories) to determine their temperature. The flue gas and the solids are coupled at the flue wall, interacting with heat flux or temperature boundary conditions. Sub-models are used to calculate the volatile release from the anodes, air infiltration/exfiltration through the top of the furnace and heat losses to environment and foundation. The furnace is treated as a counterflow heat exchanger where the gas is flowing from blowing ramp to exhaust ramp and the solids are "marching" in the opposite way at the average displacement speed of the equipment on the furnace (blower ramps, burner ramps, exhaust ramp, etc.). A complete description of that kind of model and underlying algorithm can be found in Ref. [3]. The process models are computationally cheap and give the whole portrait of the baking cycle with the help of just a few boundary conditions needed at each end of the furnace. Their shortcoming is that they do not provide detailed results of the anode baking in space and time. In particular, they do not provide a tridimensional temperature portrait of the anode stack in the pit, and the flow in the flue channel is largely simplified to that in an equivalent duct. Nevertheless, with the always increasing performance of computers, the flue gas flow can be modeled as a two-dimensional duct flow as described recently in [4].

The design models are two or tridimensional models that aim at capturing the space and time variations of the most important phenomena that take place during the baking process: convective, diffusive and radiative heat transfer, combustion of natural gas (or fuel) and volatiles in the flue channel, distribution of the turbulent gas flow in the flue channel, evolution of key anode properties, etc. Instead of including the geometry of the whole baking cycle in the model, which would be computationally expensive, the design models only include one stack of anodes and the corresponding coke, refractories and flue channel. Symmetry planes are presumed at the center planes of the anodes and flue channel. The design models consist mainly in a set of coupled partial differential equations for the gas and solids: continuity equation, momentum equations, turbulence model, species transport equations (the number of species depending on the complexity of the combustion model, typically 4-6 species), energy equation, radiation model and pitch pyrolysis kinetics equations. These models rely mostly on known boundary conditions at the inlet of the flue channel which are usually obtained with the help of a process model for the whole

baking cycle, but can also be obtained through measurement campaigns in the furnace. This kind of model is necessary in order to optimize the geometry of a furnace or a detailed operational condition of the furnace (e.g., adjust the flame length at the burners). The shortcoming of the design models is their significant computational requirements, especially if implemented in three dimensions since the model can easily contain over 10 unknown variables to solve. A typical example of a tridimensional design model can be found in Ref. [5].

Combustion modeling is a crucial aspect of a design model. In the past, authors have used either the Eddy-Dissipation model [5], which is an Arrhenius based combustion model modified for turbulence [6], [7], or a combination of the Eddy-Dissipation model with an Arrhenius reaction rate [8] in order to model combustion in ABFs. Other non-premixed combustion approaches (i.e., where fuel and oxidizer enter at separate inlets) have not been compared to the mentioned approaches. Since the energy supplied by the burning of fuel represents approximately 50-60 % of the baking energy (the remaining 40-50 % being released from the combustion of the anode volatiles), it is expected that the modeling approach is influential on the outputs of a design model.

In this paper, we examine two different approaches that have not yet been used in ABF models: first, a simplified "in-house" approach mimicking combustion is proposed, and second, the possibility to use the mixture fraction/probability density function (PDF) combustion model is evaluated. We compare the results obtained with the help of these two methods to those obtained with the Eddy-Dissipation model. Advantages and disadvantages of the three approaches will be discussed (i.e., complexity of models, convergence, flexibility, predictive potential, etc.). Additionally, variations of these models are tested, in particular the impact of radiative heat transfer in the flue channel, the significance of the diffusion term in the energy equation of the gas phase and the influence of the buoyancy terms in the momentum and turbulent kinetic energy equations.

2. Description of the anode baking furnace

A typical anode baking furnace is shown in Fig. 1. The furnace is composed of many sections, all of which are made of parallel flue channels and pits. In each flue, baffles and tie-bricks are used to deviate the flow and maintain a certain degree of uniformity in terms of heat transfer coefficients and temperature history for each anode located in adjacent pits. Each parallel flue channel in a given section is connected in series to the upstream and downstream flue channels, forming a long

channel from the blowing ramp to the exhaust ramp. Parallel flue channels are not connected together, they are independent, except at both ends of the furnace where the gas of each flue channel mixes in the crossover channel in order to reach the other side of the furnace. The furnace looks somewhat like a counter-flow heat exchanger in which gases flow on one side, and the anodes, on the other side. In practice, however, instead of moving the anodes, it is the firing equipment and blower ramps that are moved periodically from one section to the next, all sections being connected in series and forming a loop.

Figure 2 depicts a typical configuration of a fire comprising an exhaust ramp, burner ramps, blowing ramps, and pressure/temperature measurement ramps, accompanied by the corresponding typical temperature and pressure profiles in the solid and gas phases. Starting from the blowing ramp, ~~the~~ cooling air is first heated by recovering heat from the solids. This corresponds to the cooling sections of the baking cycle. Then, air is heated with the help of burners and of the combustion of volatiles released from the anodes in the heating and preheating sections, respectively. The ramps on the furnace are typically moved once a day so that the heat wave in the furnace is displaced and the anodes undergo a proper baking cycle curve with preheating, heating and cooling. This type of furnace is called an open-top horizontal ring furnace. The “open-top” means that there is no cover on the furnace, the anodes are stacked in the pits and just covered with coke for support and protection against oxidation with ambient air. The word “horizontal” refers to the overall direction of the gas flow from section to section in the furnace [9], and “ring” describes the looping pattern of the heat wave in the furnace and the displacement in circle of the equipment ramps on the furnace.

From the point of view of the anodes, the overall baking process begins in a section of the furnace where the green anodes are packed. During the first 3 following days (typically), especially when the anodes are between 200 to 600°C, volatiles are released from the binding pitch in the anodes and are transported in the flue due to the porous nature of the anodes, coke and refractory bricks. These volatiles burn in the flue, and as a consequence, anodes are preheated. The anode devolatilization has to be controlled with a heat-up rate below 15°C/h in order to prevent structural damage in the anodes, which could then affect key anode properties like flexural strength or electrical resistivity [1]. As mentioned previously, the energy supplied by the combustion of the volatiles represents about 40-50 % of the energy source in the furnace, the remaining 50-60 % being provided by the fuel at the burners [1]. The exhaust ramp that redirects the flue gas to the

gas treatment plant ensures that the pressure is below one atmosphere in order to keep all combustion products in the flues in the preheating section. The anode temperature increases from room temperature to about 700-750°C throughout the preheating.

During the second step of the baking process, which lasts approximately three more days, the heat input to the anodes comes from the combustion of natural gas (or oil) in the flue and the heat recuperated by the flue gas from the solids in the upstream cooling sections. This step is where the anodes will reach their maximal temperature of about 1100°C and corresponds to the section of interest to the present paper. Each anode undergoes a soaking time that is very important for the coking of the pitch binder matrix and the uniformity of the anodes. This maximum temperature plateau is also necessary to ensure that the heat is diffused properly in colder areas of the pit. Typically, the flue gas will be ramped up from 950 to 1200°C in the first heating section and is then kept at that maximum value in the 2 other heating sections.

Finally, the last part of the baking process is the cooling of the anodes (~5-6 days). Incoming air is preheated by the heat released from the baked anodes and other solids, which helps to reduce the amount of combustible consumed by the burners in the second step. The anodes are cooled to temperatures below 300°C in order to prevent air burn and mechanical damage when unloaded and moved to the final fabrication step, namely the rodding.

As mentioned previously, the firing system is responsible for heating the air flowing from the upstream cooling sections so that the anodes reach their maximum temperature in the firing sections. There are typically three fire ramps in a fire, and each fire ramp contains two burners per flue channel in order to distribute evenly the heat in the channel (Fig. 2), and thereby in the adjacent solids. All the ramps are moved after a period of about 24 hours in the gas flow direction, pushing forward the heat wave in the furnace. Fuel injection in the furnace is controlled by an automatic firing control system that targets an ideal baking curve. The fuel mass flow rate varies depending on the thermocouples readings downstream in the flue channel in order to match the prescribed curve. The baking curve is specific for a given furnace and depends on many factors: furnace geometry, anode raw materials, furnace conditions, production schedule, anode performance in potrooms, etc. The flames produced by the burners are, of course, in the top portion of the channel so that the refractories in that region are exposed to more thermal stresses. The hot spots created by the flames can cause flue wall cracking and therefore have a strong influence on the furnace maintenance costs with respect to the deterioration of the flue wall refractories [1]. The flames

have to be aligned in the center of the rather thin flue channels (~ 0.3 m width), otherwise they would touch the flue walls and deteriorate the refractories at an accelerated pace. For example, if natural gas is used and the composition is assumed to be 100 % methane, the stoichiometric reaction of methane with air at a temperature over 1000°C (as in the furnace) produces an adiabatic flame temperature over 2200°C [10]. The maximum service temperature of furnace refractories is around 1400-1500°C, although it is strongly recommended to keep temperature of the refractories below 1300°C [1], [11]. Therefore, it is of prime importance to control adequately the flames in the flue.

3. Common aspects to all models considered in this paper

Three approaches were used to model the effect of the burners in the anode baking furnace: a simplified 'hot gas' approach and two combustion models, namely the Eddy-Dissipation model and the mixture fraction/PDF approach. All three approaches share common geometry, mesh and equations that are described in the following sections.

3.1 Geometry

To limit the computational time, a single pit containing 18 anodes with its corresponding flue channel was modeled. This domain is sufficient to represent the whole baking cycle as experienced by the majority of the anodes in the baking furnace. Since a section of the furnace consists in adjacent flues and pits where the baking conditions are expected to be the same, it is presumed that there is a symmetry plane at the center of a flue channel, and another symmetry plane at the center of a pit (Fig. 3).

3.2 Mesh

The mesh is composed of approximately 200,000 hexahedral cells disposed orthogonally (Fig. 3). The mesh is finer in the upper region of the flue channel where important gradients of temperature and species concentrations occur because of the burners flames. The mesh is also refined in the regions of important flow gradients in the flue channel where the flue gas makes 180° turns (i.e. at the baffle-cuts). The layer of mesh along the wall of refractories is kept "thick" in the normal direction from the wall in order to use a logarithmic wall function as much as possible in the turbulence model (Section 3.4). The hexahedral cells had a typical edge size of 40 mm. The mesh was refined to a typical edge size of 20 mm for mesh independence verification. The results with the refined mesh, composed of ~950,000 cells, showed no significant difference. The main

quantity of interest from the model is the temperature of the product, i.e. the anode temperature, and the maximum relative temperature difference was very low:

$$\text{Relative difference} = \frac{\left|T_{coarse} - T_{fine}\right|}{T_{coarse}} \leq 0.35\ \% \tag{1}$$

The relative temperature difference of the flue wall (along which the gas of the flue channel exchanges heat with the refractories and the solids) is also very low being inferior to 0.9 %. In the flue channel, the refined mesh produced smoother flame profiles but the size and locations were very similar. The flue gas velocity distribution was also slightly different, a little more detailed around the corners and in the small openings, but produced no significant difference. Figure 4 shows that the high and low velocity zones were of the same size and located in the same regions of the flue channel. Considering that the flow features and the predicted temperatures were very similar with the coarse and the refined mesh, the coarse mesh is considered sufficiently fine and was preferred in order to keep the computational time acceptable.

3.3 Transport and thermophysical properties

The air entering the flue channel corresponds to 99.6 % of the mass inflow. Therefore, for simplicity, viscosity and thermal conductivity corresponding to those of air, varying with temperature, were used. Heat capacity of the gas mixture is a mass-weighted average of the individual species heat capacities, the latter being polynomial functions of temperature:

$$C_p = \sum_{i=1}^{N} \left(y_i C_{p,i} \right) \tag{2}$$

When the Eddy-Dissipation model or the “hot gas” approach are used, the density of the gas mixture is calculated via the ideal gas law:

$$\rho = \frac{p}{R_u T \sum_{i=1}^{N} \left(y_i / M_i \right)} \tag{3}$$

When the mixture fraction/PDF approach is used, the density of the gas depends on the local mixture fraction.

3.4 Gas phase governing equations

Although steady-state equations could be used in the flue channel because the thermal inertia of the gas is very small compared to that of the solids, all the equations of the present models are transient. This decision was taken because the complete model includes both the gas and solid domains, the latter requiring transient equations. The Reynolds-Averaged Navier-Stokes equations were used to calculate the averaged velocities and pressure of the turbulent flow in the flue channel. The continuity equation considers a variable density:

$$\frac{\partial \rho}{\partial t} + \frac{\partial \rho u_i}{\partial x_i} = 0 \tag{4}$$

The Boussinesq eddy-viscosity assumption is introduced in the momentum equations in order to model the Reynolds stresses associated with turbulence [12]:

$$\frac{\partial \rho u_i}{\partial t} + \frac{\partial \rho u_i u_j}{\partial x_j} = -\frac{\partial p}{\partial x_i} + \frac{\partial}{\partial x_i}\left[(\mu + \mu_t)\left(\frac{\partial u_i}{\partial x_j} + \frac{\partial u_j}{\partial x_i} - \frac{2}{3}\delta_{ij}\frac{\partial u_l}{\partial x_l} \right) \right] - \frac{2}{3}\delta_{ij}\frac{\partial \rho k}{\partial x_j} + (\rho - \rho_0)\vec{g} \tag{5}$$

The last term in Eq. (5) is included when buoyancy in the flue gas is considered, ρ is the local gas density and ρ_0 is the average gas density in the flue channel. Turbulence is modeled with the two-equation realizable k-ε model [13], which provides substantial improvement over the widely used standard k-ε model [13–16] and likely to perform better for flow impinging on surfaces (baffles and tie bricks in flue channel) [17]. In this model, the turbulent kinetic energy equation is the same as in the standard k-ε model:

$$\frac{\partial \rho k}{\partial t} + \frac{\partial \rho k u_i}{\partial x_i} = \frac{\partial}{\partial x_i}\left[\left(\mu + \frac{\mu_t}{\sigma_k} \right)\frac{\partial k}{\partial x_i} \right] + P_k + P_b - \rho\varepsilon \tag{6}$$

where P_k is the production of turbulent kinetic energy related to the rate-of-strain tensor and P_b is the production of turbulent kinetic energy due to buoyancy (if enabled in Eq. (5)). The details of these terms can be found in Ref. [12]. The last term, $\rho\varepsilon$, is the dissipation of turbulent kinetic energy by viscous stresses. The dissipation rate equation is different from that in the standard k-ε model:

$$\frac{\partial \rho \varepsilon}{\partial t} + \frac{\partial \rho \varepsilon u_i}{\partial x_i} = \frac{\partial}{\partial x_i}\left[\left(\mu + \frac{\mu_t}{\sigma_\varepsilon} \right)\frac{\partial \varepsilon}{\partial x_i} \right] + C_1 S \rho\varepsilon - C_2 \frac{\rho\varepsilon^2}{k + (\nu\varepsilon)^{0.5}} \tag{7}$$

The last two terms are production and destruction of turbulent energy dissipation (ε). Compared to the standard k-ε model, the turbulent viscosity (μ_t) is now formulated in a way that the normal

stresses cannot be negative, hence the model designation ‘realizable’. The values of the constants (σ_k, σ_ε, C_1, and C_2) in Eq. (6) and (7) are detailed in Ref. [12].

The heat is exchanged between the gas mixture and the charge (anode, coke and refractories) along the refractories wall in the flue channel. An enhanced wall-treatment approach is used to calculate the heat exchange at this interface. This approach uses a linear wall function if the y^+ values are below 11.2, and a standard logarithmic wall function if the y^+ is above 30. In between, a function blends the linear and the logarithmic functions [12]. This approach was chosen as the best compromise to deal with some regions of the flue channel where the velocity is low, especially along the baffles after the gas made a 180° turn (see Fig. 4).

The sensible enthalpy form of the energy equation is used in the Hot gas approach (section 4.1) and the Eddy-Dissipation model (section 4.2):

$$\frac{\partial \rho h_s}{\partial t} + \frac{\partial \rho u_i h_s}{\partial x_i} = \frac{\partial}{\partial x_i}\left[\left(\lambda + \frac{C_p \mu_t}{\mathrm{Pr}_t}\right)\frac{\partial T}{\partial x_i} + \sum_j h_{s,j}\left(\rho D_{j,m} + \frac{\mu_t}{\mathrm{Sc}_t}\right)\frac{\partial y_j}{\partial x_i}\right] + \dot{Q}_{rad} + \dot{Q}_{comb} \tag{8}$$

where h_s is the sensible enthalpy of an ideal gas:

$$h_s = \sum_{i=1}^{N} y_i h_{s,i} = \sum_{i=1}^{N} y_i \int_{T_{ref}}^{T} C_{p,i} dT = \int_{T_{ref}}^{T} C_p dT \tag{9}$$

The last two terms in Eq. (8) are source terms from radiation and combustion. The Hot gas approach includes solely the radiation source term, whereas the Eddy-Dissipation Model includes both terms. The specific enthalpy form of the energy equation is used with the mixture fraction/PDF approach (section 4.2):

$$\frac{\partial \rho h}{\partial t} + \frac{\partial \rho u_i h}{\partial x_i} = \frac{\partial}{\partial x_i}\left(\frac{\mu_t}{\mathrm{Pr}_t}\frac{\partial h}{\partial x_i}\right) + \dot{Q}_{rad} \tag{10}$$

where h is the specific enthalpy including the sensible enthalpy and the enthalpy of formation:

$$h = \sum_{i=1}^{N} y_i h_i = \sum_{i=1}^{N} y_i \left(\int_{T_{ref}}^{T} C_{p,i} dT + \Delta h_{f,i}^0\right) = \int_{T_{ref}}^{T} C_p dT + \sum_{i=1}^{N} y_i \Delta h_{f,i}^0 \tag{11}$$

The Finite Volume Method (FVM), a modification of the Discrete Ordinates Method (DOM) that ensures the conservation of radiant energy [18], is used to account for thermal radiation in the flue channel, the gases being treated as a participating medium. The following form of the radiative transfer equation (RTE) for an absorbing and emitting medium is solved:

$$\frac{dI(\vec{r}, \vec{s})}{ds} = \kappa(\vec{r})\left(\frac{\sigma T^4}{\pi} - I(\vec{r}, \vec{s})\right) \tag{12}$$

$I(\vec{r},\vec{s})$ is the radiative intensity at position $\vec{r}$ in direction $\vec{s}$, ds denotes the path length and $\kappa(\vec{r})$ is the local absorption coefficient. This coefficient is calculated using the weighted sum of gray gases model. It assumes a gas consisting of several gray gases, a compromise between an accurate radiation modeling and a computational effort, which makes it popular for engineering applications [19]. Two gray gases, CO_2 and H_2O, are considered in the calculation of the absorption coefficient for the Eddy-Dissipation model and the mixture fraction/PDF approach, whereas the concentration of hot gas is used in the hot gas approach. The number of directions for which Eq. (12) is solved depends on the angular discretization. In our case, the sphere of solid angles around a cell is discretized into 32 control angles. Once the radiative intensity is known in each direction, it is integrated over all control angles of a volume element. The source term in the energy equation is then

$$\dot{Q}_{rad} = \kappa\left(\vec{r}\right)\left(\int_{4\pi} I\left(\vec{r},\vec{s}\right)d\Omega - 4\sigma T^4\right) \tag{13}$$

where $I(\vec{r},\vec{s})$ is integrated over all control angles Ω and the second term represents the emitted radiation from the volume element. The same boundary condition is applied at the baffles and refractory surface for the RTE: it assumes diffusive walls with an emissivity of 1. The incident radiative heat flux is integrated over all incoming control angles, whereas the radiant intensity leaving the surface is given by the Stefan–Boltzmann law.

3.5 Solid phase equation

In the solids (anodes, coke and refractories), only the heat diffusion equation is solved:

$$\rho\frac{\partial h_s}{dt} = \frac{\partial}{\partial x_i}\left(\lambda\frac{\partial T}{\partial x_i}\right) \tag{14}$$

Each solid has a constant density, whereas the thermal conductivities and the specific heat capacities are polynomial functions of temperature from data in [1], [20]. The anodes do not release volatiles in the firing sections of the furnace, therefore there is no heat of reaction due to pitch pyrolysis included in the energy equation.

3.6 Initial and boundary conditions

Three days of firing are simulated, representing the fourth day to the sixth of a typical anode baking cycle. At the beginning of the fourth day, it is known that temperature gradients exist in the anodes. However, no sufficient data was available to define a detailed temperature profile in the anodes after preheating. Therefore, it was decided to use an initial uniform temperature of 750°C

corresponding to the average temperature after preheating. The initial air temperature in the flue channel is 1050°C. The temperature at the flue channel inlets rises linearly from 1050 to 1200°C during the first 24 h of firing, and then is maintained at 1200°C for a day. For the last day of firing, the temperature decreases linearly from 1200°C to 1100°C. The incoming flow rate of air is kept constant at 0.3 kg/s in the flue channel. The natural gas flow rate prescribed at the burner inlets is set constant at 6.5×10^{-4} kg/s for each burner, according to plant consumption data averaged over 3 days. For the hot gas approach (Section 4.1), a mass flow rate of hot gas is prescribed at 3.24×10^{-3} kg/s at each burner inlet instead of methane. Symmetry conditions are imposed at the center of the channel and center of the pit, as explained in Section 3.1. All other boundaries in the flue channel and the pit are adiabatic walls, with no slip in the flue channel.

3.7 Numerical implementation

The equations were solved with Ansys Fluent, a finite volume commercial code [21]. The equations were discretized in space with an upwind second order scheme and in time with a first order implicit scheme. The scaled residuals convergence criteria were set to 10^{-3} for all variables, except for the energy and discrete ordinates equations which were set to 10^{-6}. A time step of five minutes was used, for a total of 864 time steps. Computations were performed on two quad-core Intel Xeon X5560 CPUs on the supercomputer Colosse from Université Laval, managed by Calcul Québec and Compute Canada.

4. Specificities of each approach to model combustion

As mentioned in the introduction, the main purpose of this work is to determine which approach for the flame modeling will satisfy the model needs in the simplest way. Specifically, we aim at developing a model that includes the most important phenomena taking place in the furnace (e.g., turbulence, combustion, heat transfer). Computational time is a concern and, of course, anode temperature history and therefore anode properties predictability.

4.1 Hot gas approach

In this approach, we want to verify whether it is possible to bypass the need for a combustion model in order to simulate the impact of the flames in the flue channel. Instead of using a combustion model, which inevitably adds new variables to solve, we simply inject streams of hot gas at the burner inlets in order to mimic the energy provided by the flames in the flue.

Because we want to preserve the radiative properties of the gas mixture in the flue channel, we inject an equivalent "hot gas" having the same properties as a mixture of CO_2 and H_2O, which are the combustion products of the stoichiometric one-step combustion of methane:

$$CH_4 + 2O_2 \rightarrow \underbrace{CO_2 + 2H_2O}_{\text{hot gas}} \tag{15}$$

Knowing the quantity of methane that would normally be injected in the flue channel, the mass flow rate of the gas representing the combustion products is readily calculated. Using this approach, a supplementary mass is injected in the flue channel because the oxygen contained in the combustion products of Eq. (15) normally comes from the air already present in the flue channel. In a classical combustion model, the mass of CH_4 that would be injected at the burner inlets instead of the hot gas would constitute 0.43 % of all the mass entering the flue channel, whereas with the hot gas approach, this percentage is 2.1 %. Therefore, the added mass negligibly affects the velocity in the flue channel and the heat transfer between the gas and the charge. Mass-weighted molar mass and heat capacity of the hot gas are calculated from the mass fractions of the products in Eq. (15). The absorption coefficient is calculated using the refined weighted sum of gray gases model [22]. Knowing the concentration of the hot gas at a given point, the underlying concentrations of CO_2 and H_2O are readily calculated and so is the effective absorption coefficient. For simplicity, the viscosity and thermal conductivity of air are used since its mass fraction is about 98 %.

The energy injected in the flue channel through the hot gas has to be equivalent to the energy that would be released by methane combustion. Therefore, the temperature of the hot gas injected at the burner inlets is adjusted in order to match the heat that would be released by combustion:

$$\dot{m}_{CH_4} X_{CH_4} = \dot{m}_{hotgas} h_{s,hotgas} \tag{16}$$

where $\dot{m}_{CH_4}$ and $\dot{m}_{hotgas}$ are the mass flow rates of methane and hot gas, X_{CH_4} is the heating value of methane and $h_{s,hotgas}$ is the sensible enthalpy of the hot gas. The mass flow rate of methane considered here is the one used in the combustion models. The mass flow rate of hot gas is known from Eq. (15). The heating value of methane is determined in this way: a program determines the product species that are present at chemical equilibrium when methane at 27 °C reacts stoichiometrically and adiabatically with air at 1200 °C, as in the furnace, under ambient pressure.

We obtain a list of product species whose mass fractions are over 10^{-5} and represent the following reaction:

$$\mathrm{CH_4} + 2\left(\mathrm{O_2} + 3.76\,\mathrm{N_2}\right) \rightarrow a\,\mathrm{CO_2} + b\,\mathrm{H_2O} + c\,\mathrm{N_2} + d\,\mathrm{CO} + e\,\mathrm{O_2} + f\,\mathrm{OH} + g\,\mathrm{H_2} + h\,\mathrm{NO} + i\,\mathrm{O} + j\,\mathrm{H} \tag{17}$$

The molar coefficients of the products are not detailed here for clarity. The heat of the reaction described by Eq. (17) is then calculated with

$$Q = \sum_j n_j \Delta h^0_{f,j} - \sum_j n_i \Delta h^0_{f,\mathrm{i}} \tag{18}$$

where *i* and *j* are the reactants and products respectively, *n* are the molar coefficients in Eq. (17) and Δh^0_f are the standard formation enthalpies. The heat release obtained is X_{CH_4} ~36650 kJ per kg of methane. The remaining unknown in Eq. (16) is the sensible enthalpy of the hot gas ($h_{s,hotgas}$) which needs to be adjusted. The hot gas temperature satisfying the energy balance of Eq. (16) is the temperature of the hot gas that is imposed at the burner inlets. The hot gas sensible enthalpy is a mass-weighted-average of the CO_2 and H_2O sensible enthalpies according to their mass fractions on the right side of Eq. (15). The inlet temperature of the hot gas calculated in this way is 3750°C. This approach only needs one species conservation equation for the hot gas:

$$\frac{\partial \rho y_i}{\partial t} + \frac{\partial \rho u_j y_i}{\partial x_j} = \frac{\partial}{dx_j}\left[\left(\rho D_{i,m} + \frac{\mu_t}{Sc_t}\right)\frac{\partial y_i}{dx_j}\right] \tag{19}$$

The air concentration is calculated from the requirement that the mass fractions must sum to one.

4.2 Eddy-Dissipation model

This model has been used in the past for modeling anode baking furnaces [5], [8]. The one-step, infinitely fast chemical reaction described in Eq. (15) is once again considered. Air, composed of 79% N_2 and 21% O_2, enters the flue channel and oxygen reacts with methane in stoichiometric proportions. Therefore, four species conservation equations are needed in order to solve for N–1 species (Eq. (19) for CH_4, O_2, CO_2, H_2O). The last species, namely the nitrogen, is calculated with the requirement that the mass fractions of all species must sum to one. A source term has to be added to Eq. (19) in order to account for species consumption/production. In the present model, the reaction rate of methane (expressed in kg m^{-3} s^{-1}) is limited by the smallest of the reactants concentrations [23]:

$$R_{CH_4} = \nu_{CH_4} M_{CH_4} A \rho \frac{\varepsilon}{k} \min\left(\frac{Y_{CH_4}}{\nu_{CH_4} M_{CH_4}}, \frac{Y_{O_2}}{\nu_{O_2} M_{O_2}} \right) \quad (20)$$

Reaction rates for the other species are related to the methane combustion rate:

$$R_i = \frac{\nu_i M_i}{\nu_{CH_4} M_{CH_4}} R_{CH_4} \quad (21)$$

where the quotient on the right hand side is the stoichiometric mass ratio of species i to methane, and ν_i are the stoichiometric coefficients of the reaction. Of course, reaction rates are negative for CH_4 and O_2, and positive for CO_2 and H_2O. The source of energy due to combustion in Eq. (8) is then

$$\dot{Q}_{comb} = -\sum_i \frac{h_{f,i}^0}{M_i} R_i \quad (22)$$

where h_i^0 is the enthalpy of formation of species i.

The main advantage of the Eddy-Dissipation model is its flexibility. The model can handle any number of fuel and oxydant inlets, and the inlets compositions can differ. This flexibility can be an advantage in the detailed modeling of an anode baking furnace. Even though the present study does not include the preheating of the anodes, an integrated model for the entire baking cycle, including preheating, would benefit from this flexibility of the eddy-dissipation model. As explained in Section 2, the anode stack releases volatiles that burn in the flue channel during the first 3 days of baking. This process is non-uniform and can result in multiple volatile inlets in the flue channel with different compositions. Also in the preheating phase, air infiltration occurs at the top of the furnace because of the negative pressure caused by the exhaust ramp in those sections, which can be modeled with additional air inlets. The gas mixture that arrives in a section comes from the precedent one, and in a detailed model the 3 main inlets of a flue channel may have different compositions. For all those reasons, the Eddy-Dissipation model can be convenient for a model that simulates both the preheating and heating phases of an anode baking furnace (i.e. the first ~6 days of baking).

4.3 Mixture fraction/probability-density-function approach (PDF)

Another approach for non-premixed combustion where fuel and oxidizer enter the domain at separate inlets is the mixture fraction/PDF approach. The mixture fraction is a conserved scalar

that is neither created nor destroyed within the mixture. It represents the mass of material in the local control volume having its origin from the fuel stream:

$$f = \frac{Z_i - Z_{i,oxydizer\ stream}}{Z_{i,\ fuel\ stream} - Z_{i,oxydizer\ stream}} \tag{23}$$

where Z_i is the local mass fraction of an element i, which can be evaluated also at the inlet of the oxidizer stream and at the inlet of the fuel stream. Assuming that the diffusion coefficient is the same for all species, Eq. (23) is the same for all elements. Instead of solving the transport equations for individual species, the composition, density and temperature of the fluid can be computed from the local values of the mean mixture fraction and total enthalpy by assuming chemical equilibrium [24]. Transport equations for the time-averaged mixture fraction (f) and its variance (f'^2) have to be solved in the fluid:

$$\frac{\partial \rho f}{\partial t} + \frac{\partial \rho u_i f}{\partial x_i} = \frac{\partial}{\partial x_i}\left(\frac{\mu_t}{\sigma_t}\frac{\partial f}{\partial x_i}\right) \tag{24}$$

$$\frac{\partial \rho f'^2}{\partial t} + \frac{\partial \rho u_i f'^2}{\partial x_i} = \frac{\partial}{\partial x_i}\left(\frac{\mu_t}{\sigma_t}\frac{\partial f'^2}{\partial x_i}\right) + C_g \mu_t \left(\frac{\partial f'^2}{\partial x_i}\right)^2 - C_d \rho \frac{\varepsilon}{k} f'^2 \tag{25}$$

where the empirical constants σ_t, C_g and C_d are 0.85, 2.86 and 2.0, respectively [12]. The mixture fraction variance is needed to account for the interaction of turbulence with chemistry through the help of a probability density function (PDF). The PDF expresses the probability for the instantaneous mixture fraction to assume a certain value given the time-averaged mixture fraction (f) and its variance (f'^2). In this work, the PDF shape was the beta-function.

To the authors' knowledge, this approach has not been used for modeling combustion in an anode baking furnace model. An interesting aspect of this model is that it can predict all species that are present at chemical equilibrium at the cost of only two transport equations. The non-negligible endothermic dissociation reactions of CO_2 and H_2O at high temperature (> 930°C [24]) are accounted for, whereas they were neglected in the Eddy-Dissipation model. Therefore, the mixture fraction/PDF model is susceptible to produce a flame temperature that is lower and more realistic than the one predicted by the Eddy-Dissipation model used with Eq. (15). Another advantage is that, depending on the list of species considered at equilibrium, the model can predict pollutant species, or at least give a quantitative indication of their presence in certain operational

conditions. The model is also susceptible to converge easily since the equations do not contain non-linear combustion source terms.

4.4. Combustion models summary

To summarize Section 4, the following table shows which gas phase equations are used in each model. Table 1 shows the equations for the fluid domain only. Eq. (5) is multiplied by three because of the components of the momentum equation and Eq. (19) is multiplied by the number of species to solve. In the solids, only the energy equation, Eq. (14), is solved for the three approaches.

Table 1. Summary of the gas phase equations used by each modeling approach.

Combustion approach	**Gas phase equation numbers**	**Number of variables**	**Species**
Hot gas	(4), (5)×3, (6), (7), (8), (12), (19)	9	Hot gas, Air
Eddy-Dissipation model	(4), (5)×3, (6), (7), (8), (12), (19)×4	12	O_2, N_2, CH_4, CO_2, H_2O
Mixture fraction/PDF model	(4), (5)×3, (6), (7), (10), (12), (24), (25)	10	O_2, N_2, CH_4, CO_2, H_2O, CO, H, H_2, H_2O_2, HCO, HO_2, HOCO, HONO, O, OH, O_3, CHO

5. Results

The first part of this section aims at comparing the overall performance of the 3 approaches described in Section 4. Specifically, we look at the flames produced in the flue channel with each approach, the refractories temperature predicted along the flue wall, and how each method affects the baking of the anodes in space and time. Additionally, variations of these models are discussed, including the impact of including or disregarding the following aspects: diffusion term in the energy equation, radiation model, buoyancy, and the effect of considering air properties instead of mass-weighted properties from the species concentrations.

5.1 Comparison of the three combustion modeling approaches

The following section compares the models summarized in Table 1 without buoyancy terms included in the momentum and turbulent kinetic energy equations. As shown in Fig. 5, the flame profiles of the two classical combustion models are similar in shape, whereas the hot gas approach produced thin “flames” due to the absence of chemical reaction occurring after the gas injection.

For the combustion models, the adiabatic flame temperature calculated with the maximum air temperature (1200°C) reacting stoichiometrically with methane at 27°C serves as the maximum reference temperature that should not be exceeded with the models. The simplified one-step chemistry of the eddy-dissipation model does not include the effect of dissociation reactions among the product species and resulted in a flame temperature of 2530°C, which is ~150°C higher than the adiabatic flame temperature, whereas the mixture fraction model predicted a realistic flame temperature of 2240°C.

The temperature of the flue wall refractories (the boundary between the flue gas and the solids) are known to reach a typical maximum temperature of about 1300°C during furnace operation [1], [11]. This temperature should not be exceeded in order to keep the replacement costs of the refractories to a minimum. The maximum refractory temperature achieved during the 72 hours of firing is around 1285°C for the eddy-dissipation model and the mixture fraction model. With the hot gas approach, ray effect was present due to sharp temperature gradients (thin jets of hot gas at 3750°C) and the small angular discretization that was used [18], [25]. It resulted in unphysical hot spots on the wall with a maximum temperature of 1337°C, as can be seen in Fig. 6. Although the maximum flame temperature is well over 2000°C with the three approaches, the flames do not touch the flue wall and the predicted flue wall temperatures are realistic.

The final anode temperature obtained with the 3 approaches is very similar, as can be seen in Fig. 7. Temperature ranges from 1088 to 1179°C with the eddy-dissipation model, from 1090 to 1176°C with the mixture fraction model, and from 1081 to 1169°C with the hot gas approach. The hot gas methodology explained in Section 4.1 worked relatively well in order to inject the same amount of energy in the furnace as with the combustion models. However, the small hot gas jets resulted in a colder area at the bottom right corner of the anode stack. The velocity of the jets would need to be adjusted or calibrated in order to “push” the heat towards the bottom of the flue channel and the solids.

The numerical results have been compared to actual furnace data. However, it is important to understand the limits of this validation. For example, significant variability is found in plant data depending on the raw materials, the age, conditions and position of the pit that is surveyed, etc. Furthermore, in the present simulations a uniform anode, refractories and coke initial temperature has been considered whereas in the real furnace there is a significant horizontal temperature gradient in the furnace after the 3 days of preheating (the moment at which the model

starts). According to furnace measurements, there is a temperature difference of at least 100°C between the anodes on opposite sides of the stack after the preheating. This horizontal gradient corresponds to the heat wave that travels horizontally in the furnace. The numerical results have thus been compared with furnace measurements at locations where the measured temperatures after preheating are similar to that assumed initially in the models. Figure 8 compares the measured temperature evolution at those points against the temperature obtained with the Eddy-Dissipation model at the same location. The temperature evolutions of the anodes during three different pit surveys are reported. The comparison shows that the model predicts adequately the temperature rise compared to measurements. The flat portion of the numerical curve during the first hour is due, once again, to the initial conditions and the delay needed for the heat to diffuse from the flue wall to the center plane of the anodes. Figure 8 also demonstrates clearly the variability of the temperature evolution of the anodes in a real furnace.

The Eddy-Dissipation model with 12 variables required about 20 % less computational time than the Mixture fraction/PDF approach (10 variables), but about the same time as the hot gas approach (9 variables). It is the radiative intensity equation, Eq. (12), that is slower to converge when the Mixture fraction model is used.

5.2 Effect of radiation

The calculation of the radiation heat transfer with the Finite Volume Method discussed in Section 3.4 affects significantly the calculation time, roughly doubling it compared to model without radiation. Although it is expected that radiation has an important effect on the heat distribution in the flue channel (a thin enclosure with flames), it was considered appropriate to analyze the results of the model without radiation in order to assess to what extent the computational effort associated with radiation modeling is justified. Figure 9 shows how the heat distribution in the anodes corresponds to the baffle configuration of the flue channel when radiation is not considered. In the flue channel, the heat is mainly convected and the temperature profile of the solids exhibits the zigzag pattern corresponding to the baffles. It is hard to know if the zigzag shaped temperature distribution occurs in the real furnace since the temperature is typically measured at limited number of points in the anode stack (e.g., 9 points) and 2D temperature profiles are derived by interpolating these measurements. Another important difference in the results without radiation is the cold region at the bottom of the anodes, especially the bottom right corner which is about 90°C colder than the results obtained with the model including radiation. Furnace measurements typically show

a hot region that spreads across the entire upper part of the anodes, whereas the results without radiation show a hot region mainly concentrated in an area corresponding to the third long baffle that the gas meets in the flue channel. Both for the Eddy-Dissipation and the Mixture Fraction models, the final temperature range of the anodes is about 1090-1180°C with radiation, and 1000-1150 without radiation, the latter range being rather "cold" as a final baking temperature, especially considering that the initial anode temperature was rather hot at 750°C. The total heat transfer rate is always larger at the flue channel outlets when radiation is not included and heat is going to the next section instead of having been radiated towards the solids. In the case of the Eddy-Dissipation Model, neglecting the radiation resulted in a maximum flame temperature of about 130°C higher, which tends to be even more unrealistic compared to the adiabatic flame temperature (as mentioned in Section 5.1, the Eddy-Dissipation Model with radiation already predicted maximum flame temperature ~150°C higher than adiabatic flame temperature). The Mixture fraction approach showed a maximum flame temperature about 35°C higher. Another interesting aspect of neglecting radiation is that both combustion models produced bigger flames, as can be seen in Fig. 10 for the Mixture Fraction approach, a result of the energy being mainly convected. The extension of the radiation model to a non-gray medium was not investigated in this study because Eq. (12) would need to be solved for each wavelength band, rapidly increasing the computational burden. It is known that the absorption coefficient of gases can vary strongly across the wavelengths spectrum [18], which could have a significant effect on the radiation energy source term obtained with Eq. (13).

5.3 Effect of buoyancy

The burners produce large temperature and density gradients in the flue channel, and the model predicts zones in the flue channel where the flue gas can be very slow (blue zones in Fig. 4), therefore the influence of the buoyancy terms in Eq. (5) and (6) was verified. The results showed negligible differences on the baking of the anodes (less than 1°C difference at every point and any moment of the baking). The same can be said about the velocity magnitude field in the flue channel, only subtle differences occurred (typically less than 0.4 m/s difference at every point) and the velocity distribution was very similar whether or not the buoyancy was considered. Provided that the mass flux is fixed at the channel inlets and no infiltration (or exfiltration) can occur between inlets and outlets, the flow is largely driven by the mass conservation and the buoyancy forces do not affect the velocity field nor the heat transfer from the flue gas towards the solids.

Including the buoyancy terms in the momentum and turbulent kinetic energy equations had virtually no effect on the computational time.

5.4 Effect of heat transport due to species diffusion

The diffusive term on the right-hand side of Eq. (8) (second term within the bracket) can be neglected in the Eddy-Dissipation model and the Hot gas approach. When it is not neglected, the molecular diffusivity ($D_{j,m}$) is assumed equal to the thermal diffusivity under the assumption of a Lewis number equal to 1. The same $D_{j,m}$ is used for all species and is based on the thermal properties of air at about 1100°C. In the results obtained with both approaches, the molecular diffusion part ($\rho D_{j,m}$) of the effective diffusion coefficient is of the order of 10^{-5} kg m^{-1} s^{-1} whereas the turbulent diffusion part (μ_t/Pr_t) is of the order to 10^{-3} kg m^{-1} s^{-1}. The use of a constant $D_{j,m}$ for all species is therefore justified as the turbulent diffusion dominates. Diffusive energy transport cannot be neglected in the Mixture Fraction model, it is included in the first term on the right hand side of Eq. (10), once again assuming Le = 1 for all species. Without diffusive heat transport in the Eddy-Dissipation model, the maximum flame temperature is 130°C higher. The flame and its high temperature region are slightly smaller, but the overall flame shape is similar. The increase in the maximum flame temperature affects negligibly the temperature of the refractories and, above all, the temperature of the anodes. After 72 hours of baking, over 97 % of the refractories wall in the flue channel had a temperature difference of less than ± 12°C compared to the case with energy diffusion, and 96 % of the anode stack had a temperature difference of less than ± 15°C, which is negligible in terms of final anode properties. Neglecting the diffusive heat transport in the flue channel reduced the calculation time by 5-10 % for the Eddy-Dissipation model and the Hot gas approach.

6. Conclusions and recommendations

The present study compares different modeling approaches for an anode baking furnace. Three combustion models were tested: a simplified “in-house” approach that reproduces the burners flames and two combustion models. Furthermore, the importance of radiation, heat transfer due to species diffusion and buoyancy in the models was investigated. The simulation results were compared against plant data.

All three approaches resulted in very similar final anode temperatures, i.e. similar anode baking. When compared to actual furnace data, the three models predict a temperature rise similar

to that in a real furnace. Regarding the combustion modeling, it was found that the Eddy-Dissipation model and the Mixture fraction/PDF approach produced very similar results in terms of flame shape and flame temperature, except that the Eddy-Dissipation produced flame temperature a little too high due to simplified one-step combustion chemistry. The hot gas approach predicted anode temperatures that are very close to those predicted by the combustion models, even if the "flame" shape was thinner. The boundary conditions of the hot gas jets could be adjusted in order to match the flame shape of the combustion models. The very high temperature needed at the burners inlets with the hot gas approach (3750°C) resulted in unrealistic hot spots on the flue wall refractories, caused by too coarse an angular discretization of the radiation model.

Radiation was calculated with the Finite Volume Method (an approach derived from the Discrete Ordinates Method) and it was found to significantly affect the output of the baking as well as doubling the computational time. Neglecting radiation gave final anode temperatures that were too low compared to what is expected and measured in a real furnace. Without radiation, the heat is mainly convected in the flue channel and the resulting temperature zigzag pattern seems to differ from reality. Buoyancy terms did not affect the calculation time. The effect of heat transport due to species diffusion in the Eddy-Dissipation model and the hot gas approach was negligible in terms of the anode baking.

Considering the results obtained with the three approaches, the following recommendations can be made regarding the modeling of an anode baking furnace in the firing sections:

1. When methane is considered as the fuel injected at the burner ramps, the Eddy-Dissipation model used with a simple one-step chemistry and the Mixture fraction approach predict the same temperature for all solids within a negligible difference of just a few degrees (< 5°C). The Eddy-Dissipation model could be used for its flexibility (multiple inlets having different compositions), whereas the Mixture fraction approach should be used when maximum flame temperature prediction is important (e.g. predict refractories temperature).
2. The simplified hot gas approach, which is basically a mixing model, is a good straightforward alternative if combustion models are not available. The approach predicts an anode baking curve very similar to that obtained with the two

combustion models, but the boundary conditions (gas velocity and direction) need to be fine-tuned in order to obtain similar flame shapes and heat distribution.

3. As expected for a thin enclosure with flames, radiation heat transfer has an important effect on the heat distribution in the flue channel and therefore in the solids. It should be included in an anode baking furnace model with combustion as temperature comparison with actual furnace data match the results including radiation better. Neglecting radiation is strongly susceptible to predict temperature that is too low (~100°C colder) in the bottom area of a typical anode baking furnace configuration. The use of a non-gray radiation model could be investigated as it is susceptible to strongly affect the absorption coefficient and thus the radiative energy source term in the flue channel.
4. Buoyancy in the flue channel has no effect on the output of the three approaches used in this work. Therefore it is concluded that it can be ignored without affecting the predictions in the firing sections.
5. Heat transport due to species diffusion in the flue channel can be neglected since it has a negligible effect on the overall baking prediction. Computational time can be slightly reduced in this way (~5-10 %). If maximum flame temperature and flame shape are of particular interest, it should be included since it will affect those aspects.

Acknowledgements

The authors are grateful to the Natural Sciences and Engineering Research Council of Canada (NSERC) and to Alcoa for their financial supports via an NSERC-Cooperative Research and Development (RDC) grant entitled “Improvement of smelting energy efficiency through anode production improvement”. The operation of the supercomputer used in this work is funded by the Canada Foundation for Innovation (CFI), NanoQuébec, RMGA and Fonds de recherche du Québec – Nature et technologies (FRQ-NT).

References

[1] F. Keller and P. O. Sulger, *Anode Baking - Baking of Anodes for the Aluminum Industry*. R&D Carbon Ltd., 2008.

[2] Y. Xie, D. Kocaefe, Y. Kocaefe, L. Wei, S. Zou, and A. Wu, “Correlation between Anode Recipe and Anode Properties,” *International Journal of Engineering and Innovative Technology (IJEIT)*, vol. 2, pp. 23–27, 2013.
[3] R. T. Bui, A. Charette, T. Bourgeois, and E. Dernedde, “Performance Analysis of the Ring Furnace Used for Baking Industrial Carbon Electrodes,” *The Canadian Journal of Chemical Engineering*, vol. 65, no. 1, pp. 96–101, 1987.
[4] Y. Kocaefe, N. Oumarou, M. Baiteche, D. Kocaefe, B. Morais, and M. Gagnon, “Use of Mathematical Modelling to Study the Behavior of a Horizontal Anode Baking Furnace,” *Light Metals 2013*, pp. 1139–1144, 2013.
[5] D. S. Severo, V. Gusberti, and E. C. V. Pinto, “Advanced 3D Modelling for Anode Baking Furnaces,” *Light Metals 2005*, pp. 697–702, 2005.
[6] A. Charette and Y. Kocaefe, *Le carbone dans l’industrie de l’aluminium*. Les Presses de l’aluminium (PRAL), 2012.
[7] Y. S. Kocaefe, E. Dernedde, D. Kocaefe, R. Ouellet, Q. Jiao, and W. F. Crowell, “A 3D Mathematical Model for the Horizontal Anode Baking Furnace,” *Light Metals 1996*, pp. 529–534, 1996.
[8] M. Jacobsen and M. C. Melaaen, “Numerical Simulation of the Baking of Porous Anode Carbon in a Vertical Flue Ring Furnace,” *Numerical Heat Transfer, Part A: Applications*, vol. 34, no. 6, pp. 571–598, 1998.
[9] R. T. Bui, “Computational modelling of thermophysical processes in the light metals industry,” *Revue Générale de Thermique*, vol. 36, no. 8, pp. 575–591, 1997.
[10] C. E. Baukal Jr, *Heat Transfer in Industrial Combustion*. CRC Press, 2000.
[11] D. S. Severo, V. Gusberti, P. O. Sulger, F. Keller, and M. W. Meier, “Recent Developments in Anode Baking Furnace Design,” *Light Metals 2011*, pp. 853–858, 2011.
[12] *ANSYS Fluent Theory Guide, Release 14.5*. ANSYS Inc., 2012.
[13] T.-H. Shih, W. W. Liou, A. Shabbir, Z. Yang, and J. Zhu, “A new k-ε eddy viscosity model for high reynolds number turbulent flows,” *Computers & Fluids*, vol. 24, no. 3, pp. 227–238, 1995.
[14] M. Silieti, A. J. Kassab, and E. Divo, “Film cooling effectiveness: Comparison of adiabatic and conjugate heat transfer CFD models,” *International Journal of Thermal Sciences*, vol. 48, no. 12, pp. 2237–2248, 2009.
[15] J. J. M. Smits, “Modeling of a fluid flow in an internal combustion engine,” *Graduation report TU/e, Eindhoven University of Technology*, 2006.
[16] S. Zahirovic, R. Scharler, P. Kilpinen, and I. Obernberger, “Validation of flow simulation and gas combustion sub-models for the CFD-based prediction of NOx formation in biomass grate furnaces,” *Combustion Theory and Modelling*, vol. 15, no. 1, pp. 61–87, 2010.
[17] M. Boulet, B. Marcos, C. Moresoli, and M. Dostie, “Sequential inverse method implemented into CFD software for the estimation of a radiation boundary,” *International Journal of Thermal Sciences*, vol. 51, pp. 7–15, 2012.
[18] M. F. Modest, *Radiative Heat Transfer*. Elsevier, 2013.
[19] B. Garten, F. Hunger, D. Messig, B. Stelzner, D. Trimis, and C. Hasse, “Detailed radiation modeling of a partial-oxidation flame,” *International Journal of Thermal Sciences*, vol. 87, pp. 68–84, 2015.

[20] D. S. Severo and V. Gusberti, “User-Friendly Software for Simulation of Anode Baking Furnaces,” *Proceedings of the 10th Australasian Aluminium Smelting Technology Conference*, 2011.
[21] “ANSYS Fluent, Release 14.5, ANSYS, Inc.” 2012.
[22] C. Yin, “Refined Weighted Sum of Gray Gases Model for Air-Fuel Combustion and Its Impacts,” *Energy & Fuels*, vol. 27, no. 10, pp. 6287–6294, 2013.
[23] B. F. Magnussen and B. H. Hjertager, “On mathematical modeling of turbulent combustion with special emphasis on soot formation and combustion,” *Symposium (International) on Combustion*, vol. 16, no. 1, pp. 719–729, 1977.
[24] K. K. Kuo, *Principles of Combustion*, 2nd ed. Wiley, 2005.
[25] P. J. Coelho, “The role of ray effects and false scattering on the accuracy of the standard and modified discrete ordinates methods,” *Journal of Quantitative Spectroscopy and Radiative Transfer*, vol. 73, no. 2, pp. 231–238, 2002.

Figure captions

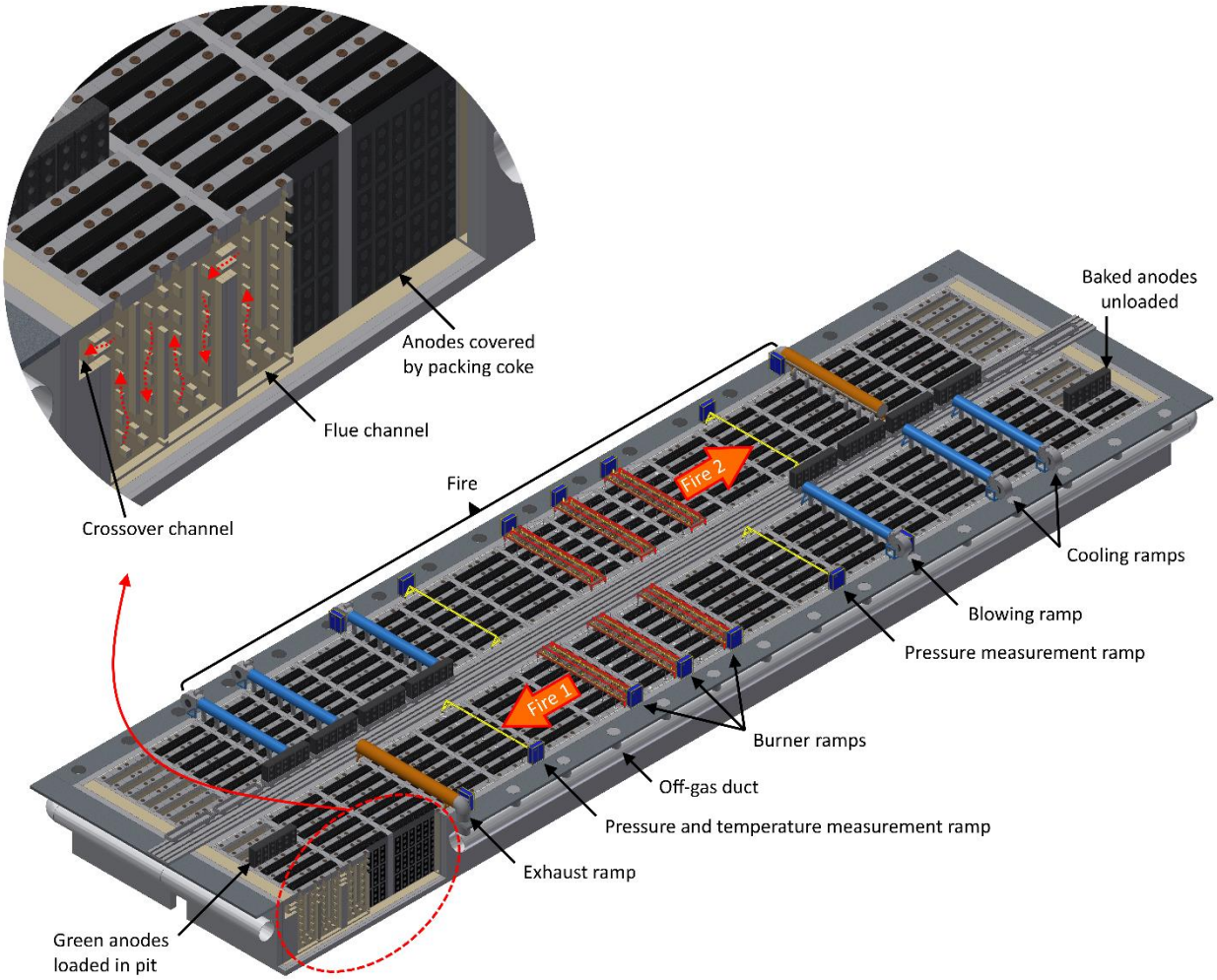

Figure 1 Schematic representation of a typical open-top horizontal anode baking furnace used in the aluminum industry.

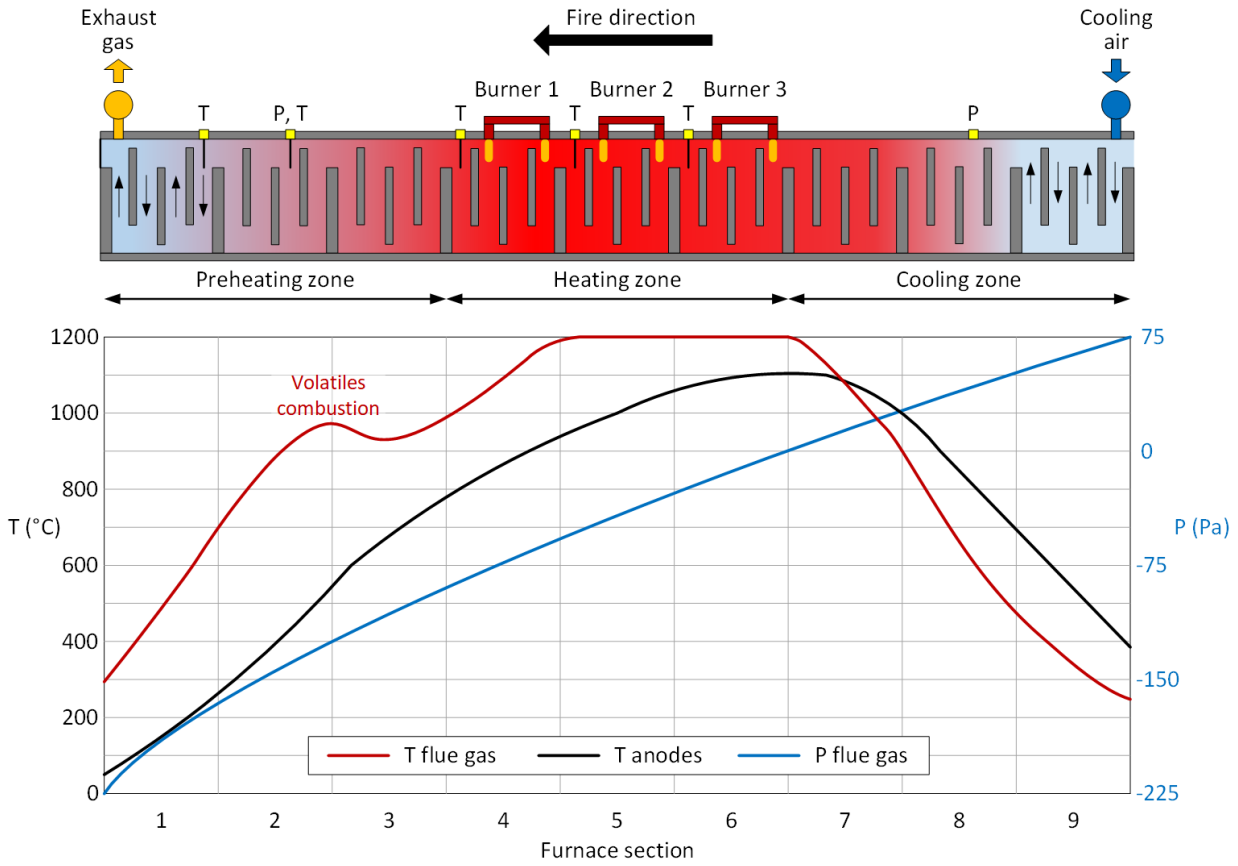

Figure 2 Average temperature of the flue gas, average temperature at the center of the anodes, and pressure of the flue gas in the corresponding sections of a fire. There is typically three more cooling sections and one more cooling ramp to cool down the anodes for safe handling and storage.

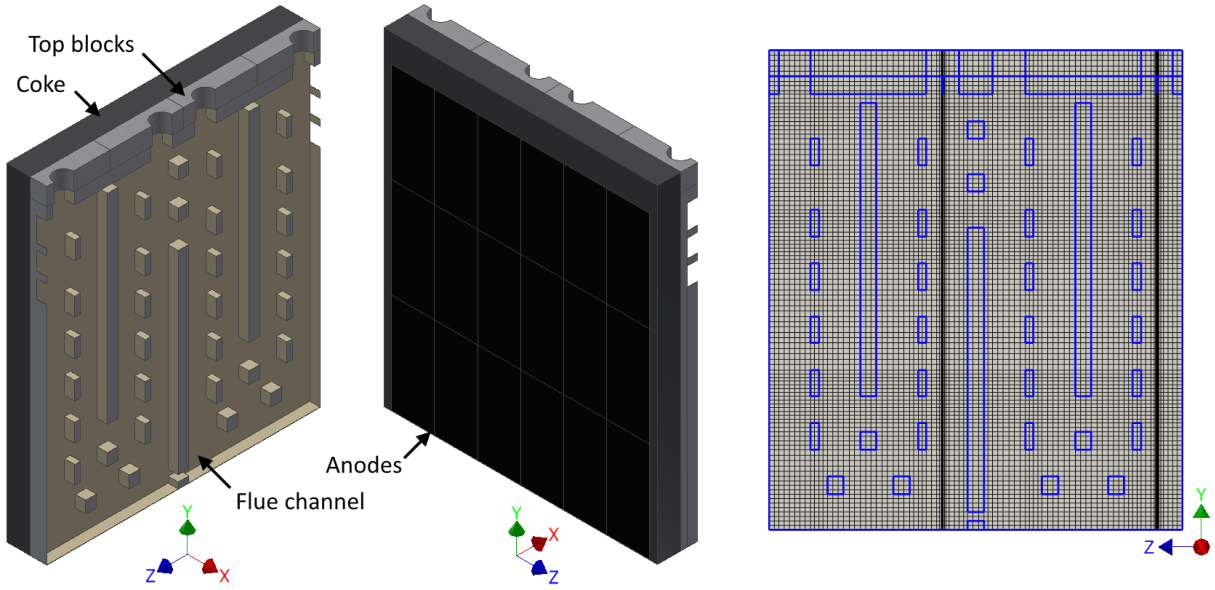

Figure 3 ½ pit and ½ flue channel domain considered in the present study (symmetry is assumed in the middle of pit and flue channel), and corresponding mesh.

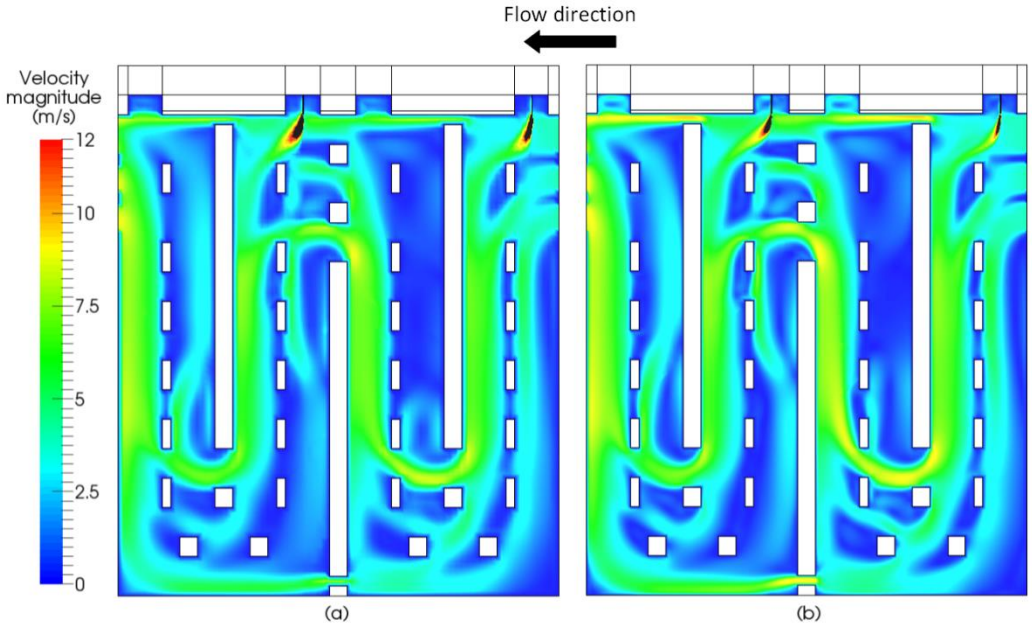

Figure 4 Velocity fields obtained with a) coarse mesh and b) fine mesh (at the symmetry axis in the channel after 72 h of firing, dark regions are out of range i.e. over 12 m/s).

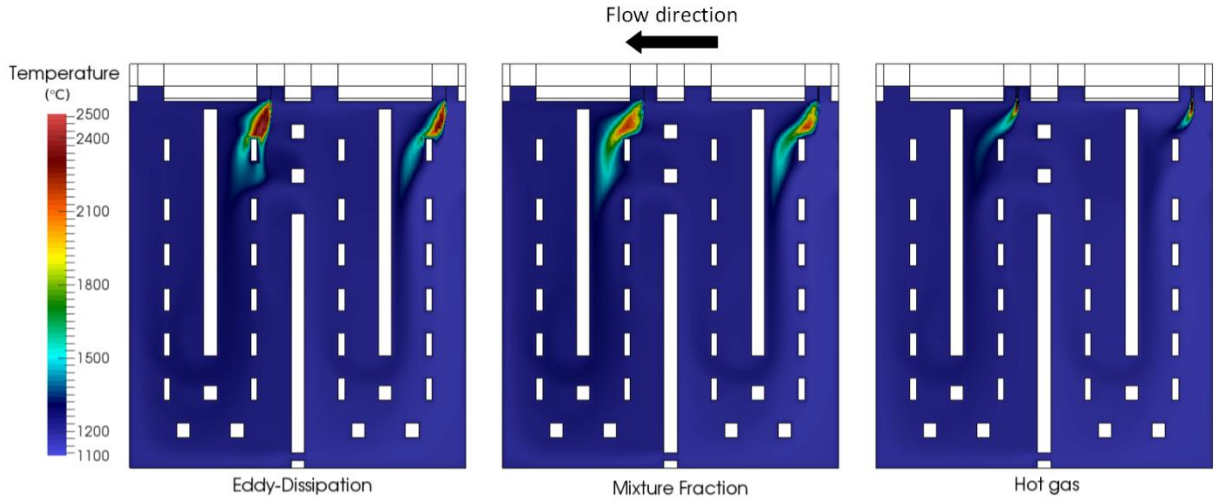

Figure 5 Comparison of the flames obtained with each approach (at the symmetry axis in the channel after 72 h of firing)

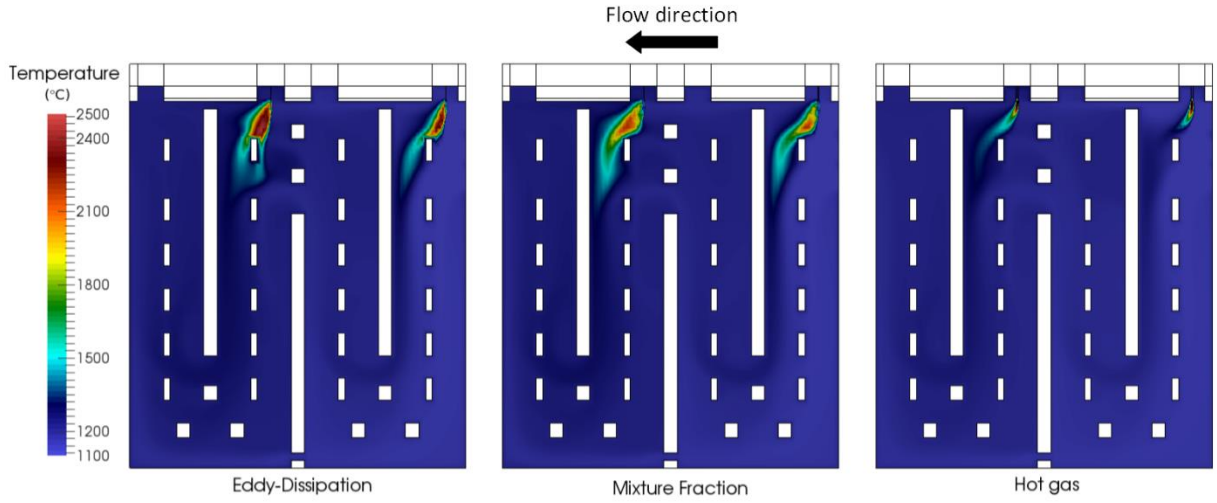

Figure 6 Comparison of the refractories temperature obtained with each approach (surface of refractories after 72 h of firing)

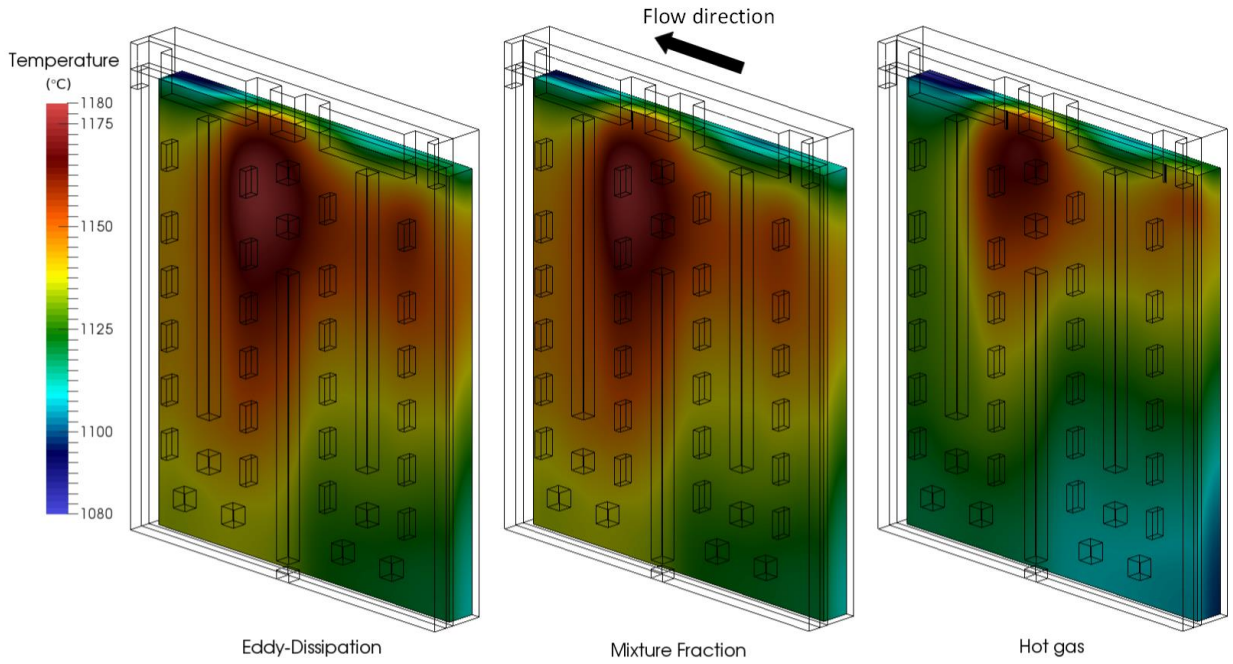

Figure 7 Comparison of the anode temperature obtained with the 3 approaches (after 72 h of firing).

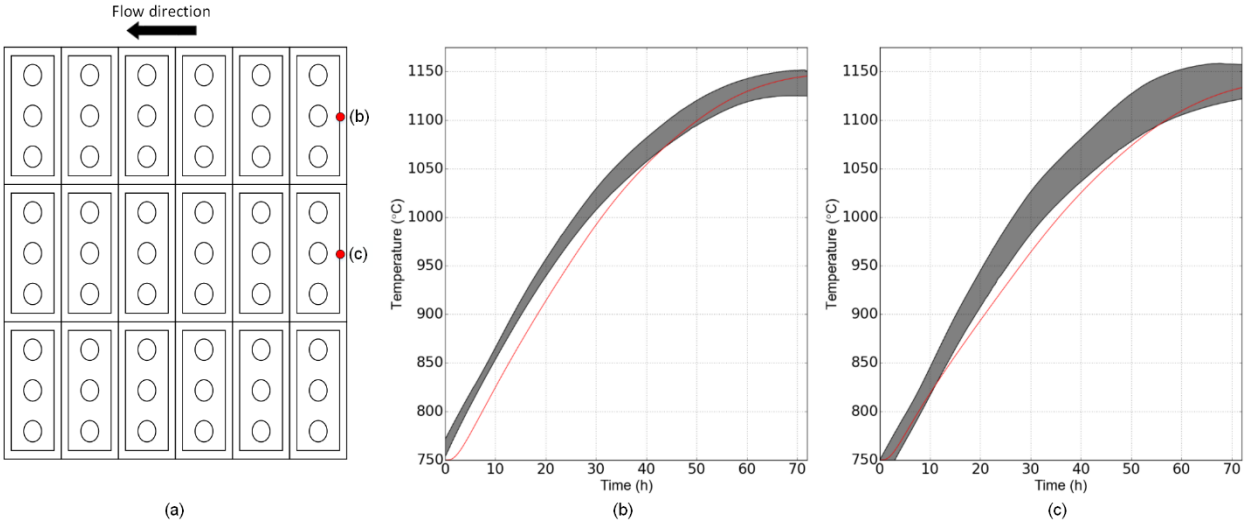

Figure 8 Comparison between model results and pit surveys data: (a) Location where temperature was measured; (b) and (c) Temperature measurement and model predictions for positions b and c as a function of time. Grey area in (b) and (c) represents the range of temperature from measurements from different pit surveys and the red curve is the output of the Eddy-Dissipation model.

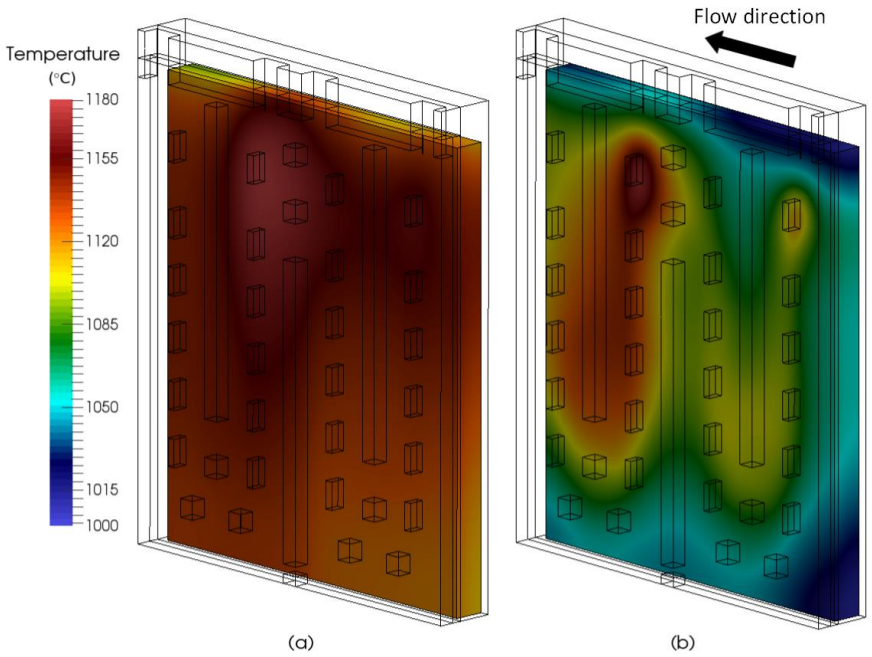

Figure 9 Comparison of the anodes temperature obtained with the Eddy-Dissipation model when a) radiation is considered in the flue and b) radiation is neglected in the flue channel (after 72 h of firing).

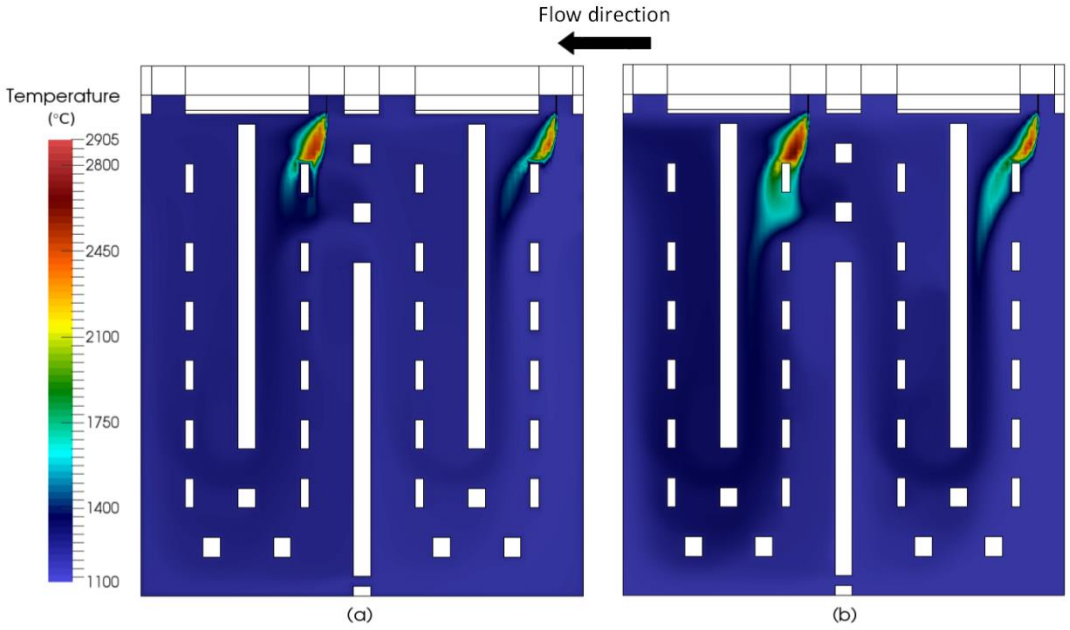

Figure 10 Comparison of the flame shape obtained with the Eddy-Dissipation model when a) radiation is considered and b) radiation is neglected (at the symmetry axis in the channel after 72 h of firing).